Journal of Materials Chemistry C

The intrinsic thermal transport property of biphenylene network and the influence of hydrogenation: A first-principles study

Journal:	*Journal of Materials Chemistry C*
Manuscript ID	TC-ART-09-2021-004154.R1
Article Type:	Paper
Date Submitted by the Author:	03-Oct-2021
Complete List of Authors:	Zhang, Pei; Xiangtan University School of Physics and Optoelectronics, Xiangtan University Ouyang, Tao; Xiangtan University, Laboratory for Quantum Engineering and Micro-Nano Energy Technology & Department of Physics Tang, Chao; Xiangtan University, School of Physics and Optoelectronics; Xiangtan University, Hunan Key Laboratory for Micro-Nano Energy Materials and Devices He, Chaoyu; Xiangtan University, School of Physics and Optoelectronics Li, Jin; Xiangtan University, Laboratory for Quantum Engineering and Micro-Nano Energy Technology Zhang, Chunxiao; Xiangtan University, Laboratory for Quantum Engineering and Micro-Nano Energy Technology Hu, Ming; University of South Carolina, Mechanical Engineering Zhong, Jianxin; Xiangtan University, Laboratory for Quantum Engineering and Micro-Nano Energy Technology

The intrinsic thermal transport property of biphenylene network and the influence of hydrogenation: A first-principles study

Pei Zhang[1], Tao Ouyang[1,a], Chao Tang[1,a], Chaoyu He[1], Jin Li[1], Chunxiao Zhang[1], Ming Hu[2,a] and Jianxin Zhong[1]

1. Hunan Key Laboratory for Micro-Nano Energy Materials & Device and School of Physics and Optoelectronics, Xiangtan University, Xiangtan 411105, Hunan, China

2. Department of Mechanical Engineering, University of South Carolina, Columbia, SC 29208, USA

Abstract: Utilizing first-principles calculations combined with phonon Boltzmann transport theory up to the fourth-order anharmonicity, we systematically investigate the thermal transport properties of biphenylene network [BPN, recently synthesized experimentally by Fan et al., Science, **372** 852-856 (2021)] and hydrogenated BPN (HBPN). The calculations show that four-phonon scattering significantly affects the lattice thermal conductivity (κ) of BPN. At room temperature, the κ of BPN is reduced from 582.32 (1257.07) W/mK to 309.56 (539.88) W/mK along the *x* (*y*) direction after considering the four-phonon scattering. Moreover, our results demonstrate that the thermal transport in BPN could also be greatly suppressed by hydrogenation, where the κ of HBPN along the *x* (*y*) direction is merely 16.62% (10.14%) of that of pristine BPN at 300 K. The mechanism causing such obvious decreasing of κ of HBPN is identified as the enhanced phonon scattering rate and reduced group velocity, which is further revealed by the increased scattering

[a] Corresponding author. E-mail: ouyangtao@xtu.edu.cn (Tao Ouyang). tang_chao@xtu.edu.cn (Chao Tang). hu@sc.edu (Ming Hu).

phase space and weakened C-C bond. The results presented in this work shed light on the intrinsic thermal transport features of BPN and HBPN, which will help us to understand the phonon transport processes and pave the way for their future developments in the thermal field.

Keywords: Biphenylene network (BPN), hydrogenated biphenylene network (HBPN), thermal conductivity, first-principles calculation, four-phonon scattering

1. Introduction

Carbon materials occupy a crucial position in the development of science and technology due to their unique properties and rich variety of allotropes [1-6]. Since the discovery of monolayer graphene [5], two-dimensional (2D) carbon materials have received extensive attention [7-9] and numerous new 2D carbon allotropes with rich electronic properties have been predicted and reported. For instance, net W [10], R-graphyne [11], ψ-graphene [12], and net-τ [13] are featured with metallic characteristics, while graphenylene [14], penta-graphene [15], twin graphene [16], and C68-graphyne [17] are semiconductors with different band gaps. More interestingly, OPG-Z [18], phagraphene [19], Stone-Wales graphene [20], and SW40 [21] are semimetals with topological properties. In addition to the advances in theory, great effort has also been made in the experimental synthesis of 2D carbon materials. Large-area graphdiyne film has been prepared by cross-coupling reaction of hexaethylbenzene [22]. By means of an on-surface reaction approach, phagraphene and TPH-graphene have been obtained as well [23]. Recently, biphenylene network (BPN), the previously predicted graphene allotropes with metallic properties, has been realized via an on-surface interpolymer dehydrofluorination reaction by Fan et al. [24]. These advancements illustrate that 2D carbon structures never cease to inspire the enthusiasm and creativity of researchers.

Thermal transport is a fundamental physical property of materials and is essential for practical applications, such as thermal dissipation in electronic devices and heat hindering in thermoelectrics. Various thermal transport properties are reported in 2D carbon allotropes, which is stimulated a wide range of research interests. The suspended graphene possesses a superb thermal conductivity (κ) of over 3000 W/mK at room temperature. Other 2D carbon structures with similar planar

configurations, however, display different thermal transport behaviors. For example, the κ of penta-graphene is about 645 W/mK [25], and that of γ-graphyne with sp and sp^2 hybrid states is merely 76 W/mK which is two orders of magnitude lower than that of graphene at 300 K [26]. These results indicate that the geometric structure and C-C bond type have an important influence on the κ of the 2D carbon allotropes. Meanwhile, it is also vital to modulate the κ to meet the needs of a variety of different application requirements. Several methods have been developed to effectively regulate the κ, e.g. nanostructuring [27, 28], introduction of pores and impurities [29, 30], and strain [31-33]. Among the various methods, recent studies on hydrogenated graphene and penta-graphene have demonstrated that hydrogenation is also a feasible way to adjust the κ of 2D materials [34, 35]. Considering the peculiar configuration arranged with tetragonal, hexagonal, and octagonal carbon rings in recent prepared BPN [24], it is natural to ask that how its distorted sp^2 hybridization bonds will affect its intrinsic thermal conductivity? How could hydrogenation modulate its thermal conductivity?

To answer these questions, in this work, we systematically investigate the κ of BPN and hydrogenated BPN (HBPN) by means of first-principles combined with phonon Boltzmann transport theory by considering both three- and four-phonon scattering. The calculations show that the four-phonon scattering plays a significant role in the intrinsic thermal transport properties of BPN and HBPN. Meanwhile, we also find that hydrogenation not only weakens the anisotropy of thermal conductivity and phonon hydrodynamics of BPN, shortens the phonon mean free path as well, but also leads to a significant decrease in κ. The rest of this paper is organized as follows. In Section 2, a brief description of computational details of first-principles and Boltzmann transport

theory is presented. In Section 3, we show the main calculation results and discuss in detail the κ of BPN and HBPN based on phonon scattering rate, group velocity, scattering phase space, and hybridization orbitals of electrons. Finally, the conclusions of this work are given in Section 4.

2. **Method**

The first-principles calculation is carried out by density functional theory employing the projector augmented wave (PAW) pseudopotential in the Vienna *ab initio* simulation package (VASP) [36-38]. Exchange-correlation functional adopts Perdew-Burke-Ernzerhof (PBE) of generalized gradient approximation (GGA) [39]. Both BPN and HBPN use a plane wave basis with cutoff energy of 550 eV, and their Brillouin zone (BZ) is sampled with 7 × 8 × 1 and 7 × 7 × 1 Monkhorst-Pack k-mesh, respectively. The energy and Hellmann-Feynman forces convergence criteria are set to 10^{-6} eV and 10^{-4} eV/Å, respectively. A vacuum region of more than 15 Å is applied for avoiding layer-to-layer interactions caused by periodic boundary conditions.

The harmonic second-order force constants and phonon spectra are computed by using VASP and PHONOPY software [40]. The anharmonic third-order force constants are generated by the thirdorder.py script and interaction up to the sixth nearest neighbors is employed [41]. The fourthorder.py code is utilized to obtain the anharmonic fourth-order force constants [42], and we consider the interaction up to the second nearest neighbors. The real-space finite-difference method and same supercell sizes are used to calculate the harmonic and anharmonic force constants, i.e., 3 × 4 × 1 and 2 × 2 × 1 supercells are taken for BPN and HBPN, respectively. We adopt the thickness

of 3.35 Å and 5.3 Å for BPN and HBPN with considering the Van der Waals radius, respectively. Based on the physical quantities obtained above, the phonon transport properties of BPN and HBPN are obtained via the ShengBTE software package [43]. The phonon thermal conductivity is defined as [43]:

$$\kappa_\alpha = \sum_\lambda c_\lambda v_{\lambda,\alpha}\left[\tau_\lambda^0\left(v_{\lambda,\alpha} + \Delta_\lambda\right)\right], \quad (1)$$

where c_λ, $v_{\lambda,\alpha}$, τ_λ^0 and Δ_λ denote specific heat, phonon group velocity along the α direction, phonon relaxation time, and correction term with the dimension of velocity, respectively, and the subscript $\lambda \equiv (q, p)$ is the sum of all phonon modes in the Brillouin zone, where *q* and *p* are the phonon wave vectors and mode indices. Both three-phonon and four-phonon scattering rates ($1/\tau_\lambda$) are considered in this work. In order to get the convergence of the thermal conductivity, phonon q-grid points of 36 × 45 × 1 (16 × 20 × 1) and 20 × 20 × 1 (6 × 6 × 1) are chosen for BPN and HBPN for considering the three-phonon (four-phonon) scattering rate, respectively (the convergent results are depicted in the Figs. S1 and S2 of supplementary information).

3. **Result and discussion**

Firstly, we give the structural information about the BPN and HBPN, where the top and side views of both BPN and HBPN are illustrated in Fig. 1. It can be seen that the BPN possesses six carbon atoms in each primitive cell, and it consists of four-, six- and eight-membered carbon rings and the optimized lattice constants of BPN are a = 4.52 Å and b = 3.76 Å, which agree well with previous theoretical and experimental results [24, 44]. The ground state configuration of the HBPN

sheet is determined by using the powerful structure search software RG2 code [45]. Detailed information about searching for HBPN sheets can be found in our recent work [46]. After the hydrogenation of BPN, the space group changes from Pmmm (No. 47) to Cmma (No. 67). Different from BPN, the HBPN hosts 24 atoms (12 carbon atoms and 12 hydrogen atoms) in each primitive cell. The optimized lattice constant of HBPN is a = b = 5.86 Å. As shown in Fig. 1(c) and 1(d), it is obvious that when the BPN is hydrogenated, the planar structure turns into a buckled configuration due to the variation of orbital hybridization form. It should be also pointed out that hydrogenation does not destroy the original C-C bond and modifies the basic atomic framework of BPN (the carbon atoms are still arranged in four, six, and eight-membered rings). However, such behavior leads to a notable difference in the electronic band structures between BPN and HBPN, i.e., the BPN is transformed from metal to insulator after hydrogenation, and the band gap of HBPN is about 4.65 eV based on the HSE06 potential (more information could be found in Fig. S3 of supplemental information).

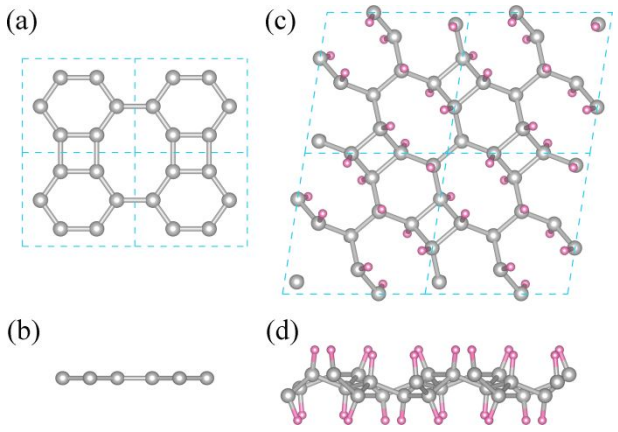

Figure 1. Top and side view of (a, b) biphenylene network (BPN) and (c, d) hydrogenated biphenylene network (HBPN). The gray and red balls denote carbon and hydrogen atoms,

respectively. The blue dashed boxes in (a) and (c) indicate the primitive cells.

Based on the optimized structure, we analyze the phonon dispersion relations to verify the dynamical stability of BPN and HBPN. Their corresponding phonon spectra and phonon density of states (*p*DOS) are depicted in Fig. 2. The phonon spectra of both BPN and HBPN are free of imaginary frequencies, indicating they are dynamically stable in the ground state. One can also find that the phonon branches in BPN become more numerous and denser after hydrogenation, which leads to a larger *p*DOS. In addition, the cutoff frequency of optical phonon branches of HBPN is 89.22 THz, which is much larger than that of BPN (49.34 THz) and mainly originated from the light mass of hydrogen atoms. However, it is worth mentioning that the phonon branches of HBPN are significantly softened in the low frequency region (less than 40 THZ). From the partial DOS shown in Fig. 2(b), it can be noted that the phonons in the low-frequency region are mainly contributed by C atoms, while the contribution from H atoms is mainly in the high-frequency phonon region. The behavior of these phonon branches will play a critical role in phonon transport, which will be discussed in the following.

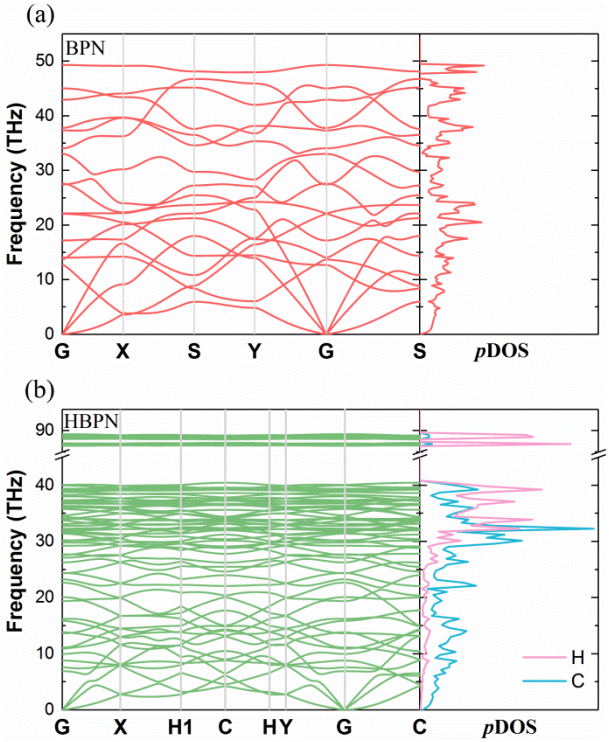

Figure 2. The phonon dispersions curve and phonon density of states (*p*DOS) of (a) BPN and (b) HBPN. For HBPN, the atom partial DOS are plotted. The coordinates of the high-symmetry points in the Brillouin zone are: G (0, 0, 0), X (0.5, 0, 0), S (0.5, 0.5, 0), Y (0, 0.5, 0), H1 (0.865, 0.433, 0), C (0.5, 0.5, 0), H (0.135, 0.568, 0).

In Figs. 3(a) and 3(b), we plot the lattice thermal conductivity as a function of temperature for both BPN and HBPN. Here, we carry out the three-phonon (3-phonon) scattering computation with the iterative method. As for the four-phonon (4-phonon) scattering processes, we utilize the relaxation time approximation (RTA) approach because the iterative way will demand large calculation resources (processor and memory), which is a comment treatment for the high-order anharmonic phonon scattering calculation [42]. Since the ascent of temperature will strengthen the

Umklapp phonon-phonon scattering, it can be seen that the κ of both BPN and HBPN decreases with increasing temperature, which is typical behavior of crystalline materials [47-49]. Meanwhile, one can notice that after including the 4-phonon scattering the κ is far lower than that with only 3-phonon scattering considered. For instance, at room temperature, the κ along the *x* (*y*) direction for BPN decreases from 582.32 (1257.07) W/mK to 309.56 (539.88) W/mK, by 46.84% (57.05%). Analogous phenomena could also be found in the HBPN. Such reduction in κ could be easily understood from the enhancement of scattering rate shown in Figs. 4(a) and 4(b). It should be mentioned here that our calculated thermal conductivity (only with 3-phonon scattering) of BPN is larger than the results reported in a recent work [44]. The discrepancy might be attributed to the different supercell sizes and cutoff radius for obtaining the harmonic and anharmonic force constants. We also notice the large anisotropy in phonon transport of BPN, i.e. the $\kappa^{3+4\,ph}$ along the *y* direction is 1.74 times higher than that along the *x* direction, which is mainly caused by the anisotropic structure of BPN. In addition, it can be viewed from Fig. S4 that the discrepancy between the thermal conductivity of BPN obtained by the iterative and RTA methods is significant. At room temperature, the difference factor $(1-\kappa_{RTA}^{3\,ph}/\kappa_{\text{Iterative}}^{3\,ph})$ along the *x* (*y*) direction is 0.48 (0.47). Such a large difference factor suggests the possible existence of phonon hydrodynamics in BPN, which is also observed in graphene [50].

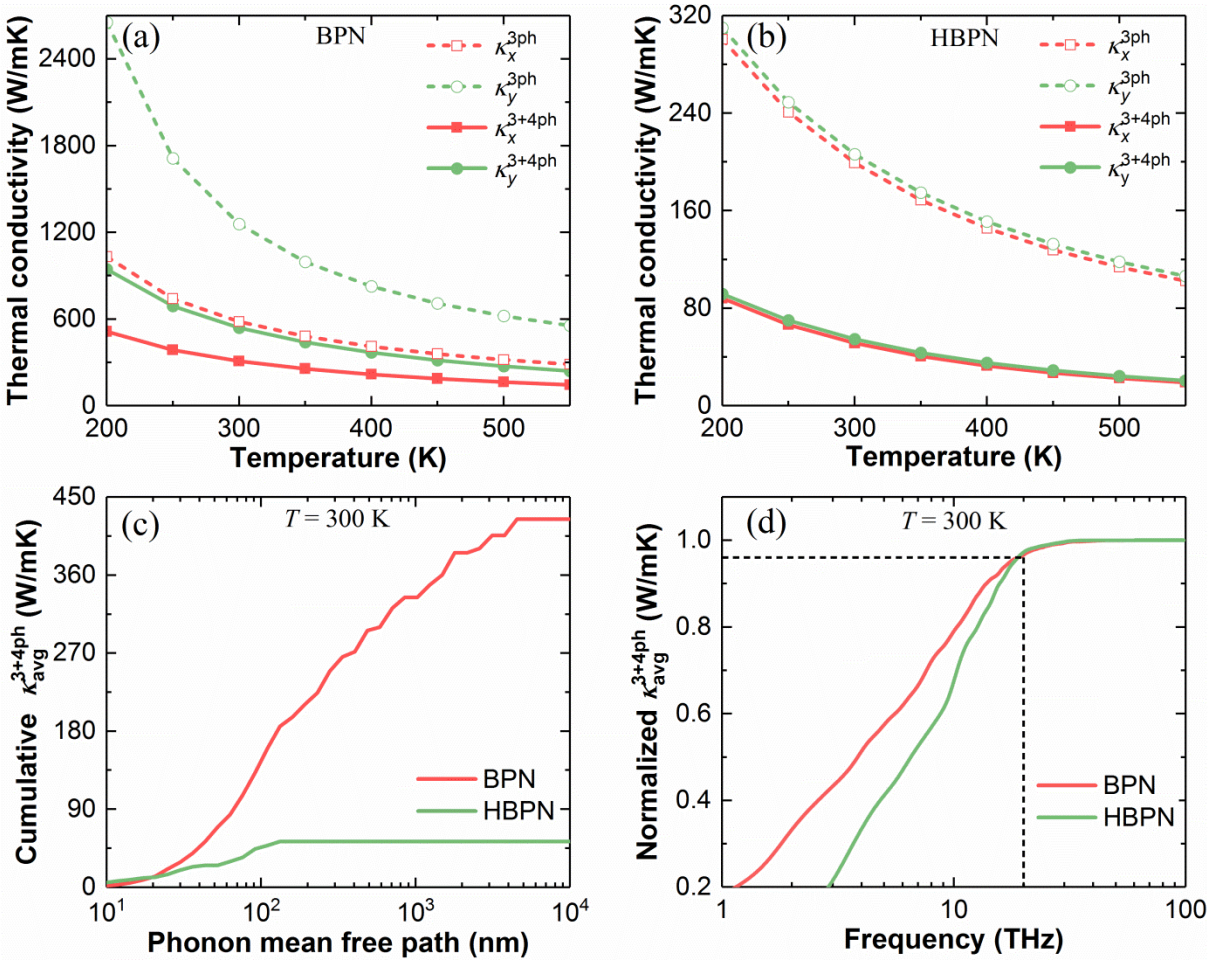

Figure 3. Thermal conductivity versus temperature for (a) BPN and (b) BPN along the *x* and *y* directions. 3ph and 3+4ph denote only three-phonon scattering and both three-phonon and four-phonon scattering, respectively. (c) Cumulative $\kappa_{\text{avg}}^{3+4\,ph}$ as a function of phonon mean free path. (d) Normalize cumulative $\kappa_{\text{avg}}^{3+4\,ph}$ as a function of frequency.

Another significant result presented in Figs. 3(a) and 3(b) is that after the BPN is hydrogenated to HBPN, its thermal conductivity is greatly suppressed. The room temperature $\kappa^{3+4\,ph}$ of HBPN along the *x* (*y*) direction is merely 51.46 (54.73) W /mK, which is only 16.62% (10.14%) of that of

BPN. Besides, the anisotropic thermal transport in BPN disappeared as well in HBPN, where the anisotropic factor $[\left|\kappa_x^{3+4ph}-\kappa_y^{3+4ph}\right|/(\kappa_x^{3+4ph}+\kappa_y^{3+4ph})]$ decreases from 0.27 to 0.03 at 300K. Interestingly, it can also be seen from Fig. S4(c) that the difference factor of HBPN is much smaller than that of BPN, e.g., at room temperature, the difference factor of HBPN is only 0.05 (0.04) along the x (y) direction. Such variation implies that hydrogenation may reduce the phonon hydrodynamics of BPN as well. For showing the effect of hydrogenation on the thermal conductivity of BPN more clearly, the cumulative averaged thermal conductivity $[\kappa_{avg}^{3+4ph}=(\kappa_x^{3+4ph}+\kappa_y^{3+4ph})/2]$ as a function of the phonon mean free path (PMFP) at room temperature is depicted in Fig. 3(c). It is evident that their $\kappa_{\mathrm{avg}}^{3+4ph}$ at first increases with the PMFP and then converges to a constant value of 424.72 W/mK and 53.10 W/mK for BPN and HBPN, respectively. Moreover, one can find that hydrogenation also causes a reduction in the PMFP, with the maximum PMFP falling from 4534.88 nm for BPN reduce to 132.19 nm for HBPN. This indicates that nanostructuring might be a more effective way to modulate the thermal conductivity of HBPN. Finally, we also give the $\kappa_{\mathrm{avg}}^{3+4ph}$ as a function of phonon frequency. It can be noted from Fig. 3(d) that most of the $\kappa_{\mathrm{avg}}^{3+4ph}$ is contributed by phonons with frequencies below 20 THz for both BPN and HBPN.

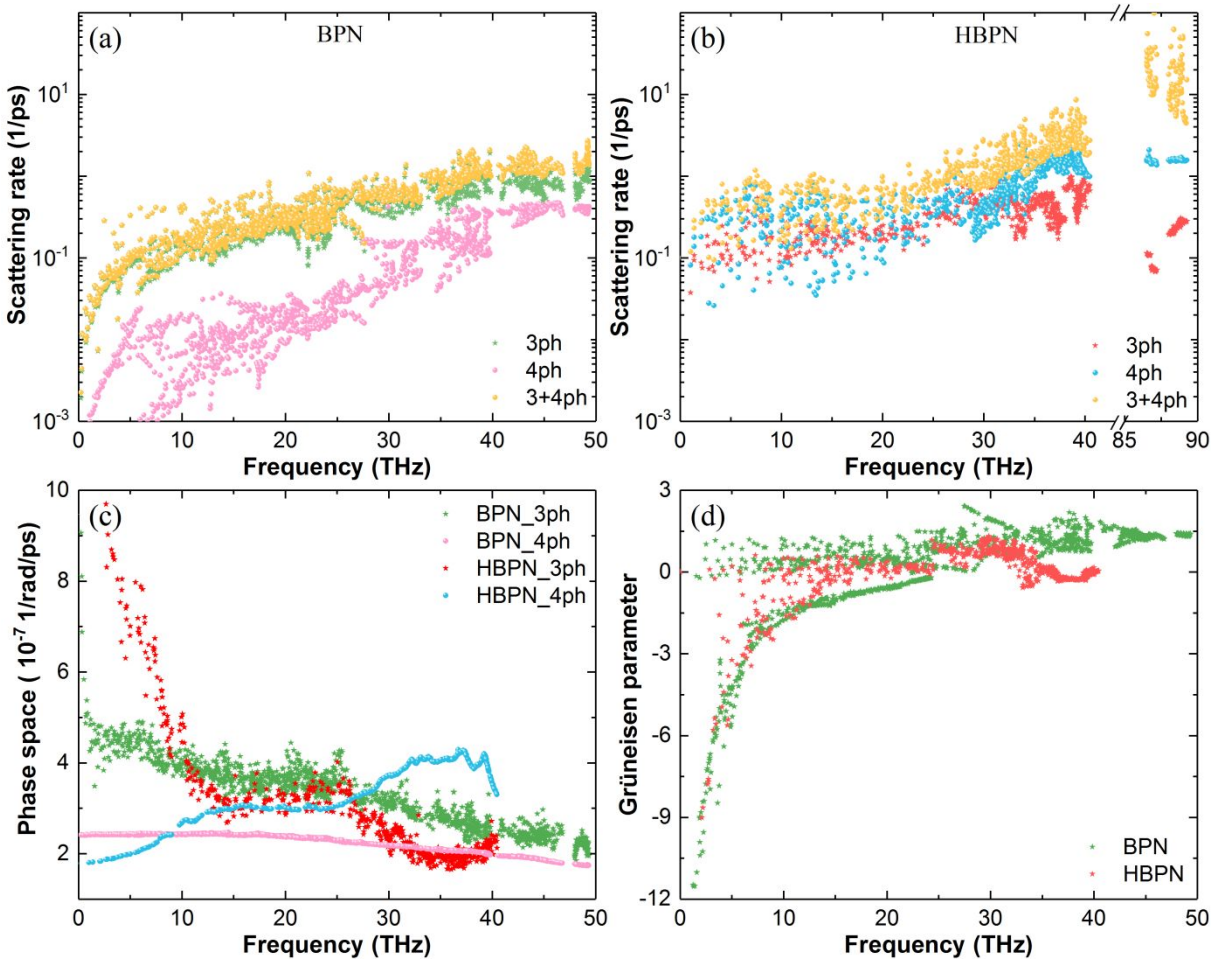

Figure 4. At room temperature, comparison of phonon scattering rate of (a) BPN and (b) HBPN. 3ph, 4ph, and 3+4ph denote only 3-phonon scattering, 4-phonon scattering, and both 3-phonon and 4-phonon scattering, respectively. (c) 3-phonon and 4-phonon scattering phase space of BPN and HBPN. (d) Grüneisen parameter of BPN and HBPN.

To explore the physical mechanism of the evident reduction of $\kappa_{\mathrm{avg}}^{3+4\,ph}$ of HBPN, we decompose the phonon properties that influence the κ, i.e., specific heat (C_λ), phonon scattering rate ($1/\tau_\lambda$), and phonon group velocity (v_λ). Since the softening of phonon modes after hydrogenation leads to more phonon modes per unit frequency, as listed in Table 1, the specific heat of HBPN is

greater than that of BPN. That is to say, the elevated specific heat is not responsible for the lower κ of HBPN. As for the phonon scattering rate, it can be seen from Fig. 4(a) and 4(b) that the phonon scattering rate of HBPN is much larger than that of BPN. In other words, the phonon relaxation time is reduced, which is one of the reasons for the decrease of $\kappa_{\mathrm{avg}}^{3+4\,ph}$ after hydrogenation.

Table 1. The specific heat of BPN and HBPN

Material	BPN	HBPN
Specific heat (kJ/m^{3}K)	281.12	367.73

The phonon scattering rate is determined by two factors, one of which is the amount of phonon scattering channels, determined by the 3-phonon and 4-phonon scattering phase space. The other is the intensity of phonon scattering, which is quantified by the Grüneisen parameter. As one can observe in Fig. 4(c), the hydrogenation boosts the 3-phonon (phonon frequency < 10 THz) and 4-phonon (phonon frequency > 10 THz) scattering phase space. Such enhancement originates from the fact that the increased and softened phonon branches caused by hydrogenation make it easier for phonons to satisfy energy and quasi-momentum conservation, thereby allowing more channels for phonons to be scattered. Nevertheless, the Grüneisen parameter (absolute value) of the HBPN is lower than that of the BPN as depicted in Fig. 4(d), indicating a weaker anharmonicity of the HBPN. It is evident that the reduction in anharmonicity cannot explain the increasing phonon scattering rate of HBPN with respect to BPN. Therefore, one can conclude that it is mainly the enhancement of the scattering phase space that causes the decrease of phonon scattering rate of

HBPN compared to BPN.

According to Equation 1, the phonon group velocity is the other key factor affecting the κ. It is clearly seen from Fig. 5(a) that the group velocity of HBPN is reduced compared to that of BPN. The maximum phonon group velocity of BPN is 19.53 km/s and that of HBPN is only 13.37 km/s, and the smaller group velocity is consistent with the lower Young's modulus (Table S1). Such reduction is attributed to the softening of phonon branches with frequencies less than 40 THz mentioned earlier since group velocity is the slope of the phonon branch. As all the properties are substantially dependent on the atomic structure and electronic properties, we further investigate the group velocity from the viewpoint of bond strength. One can notice from Figs. 5(b-c) and S3(b) that the carbon atoms in BPN are bonded to only three adjacent carbon atoms and therefore form sp^2 hybridization orbitals, while the p_z orbitals are not involved in hybridization and form π-bond. After hydrogenation, the previously unhybridized p_z orbital of carbon atom hybridizes with the *s* orbital of the hydrogen atom to form the sp^3 hybridization orbital [Fig. S3(d)], which induces the buckled structure of HBPN. In general, the fewer the "s" properties of a material, the weaker its bond energy will be [35, 51]. Therefore, the strength of the C-C bond becomes weaker after hydrogenation, as evidenced by the trace of the harmonic force constant in Table S2 in the supplementary information. At the same time, the electron local function (ELF) could also demonstrate the bonding properties visually. The electrons previously in the unhybridized p_z orbital of BPN are currently localized on the C-H bond [large red areas in Fig. 5(d)] and hence are not anymore involved in C-C formation. As a result, it is the weakening of the C-C bond that leads to the decrease of the group velocity of HBPN relative to BPN.

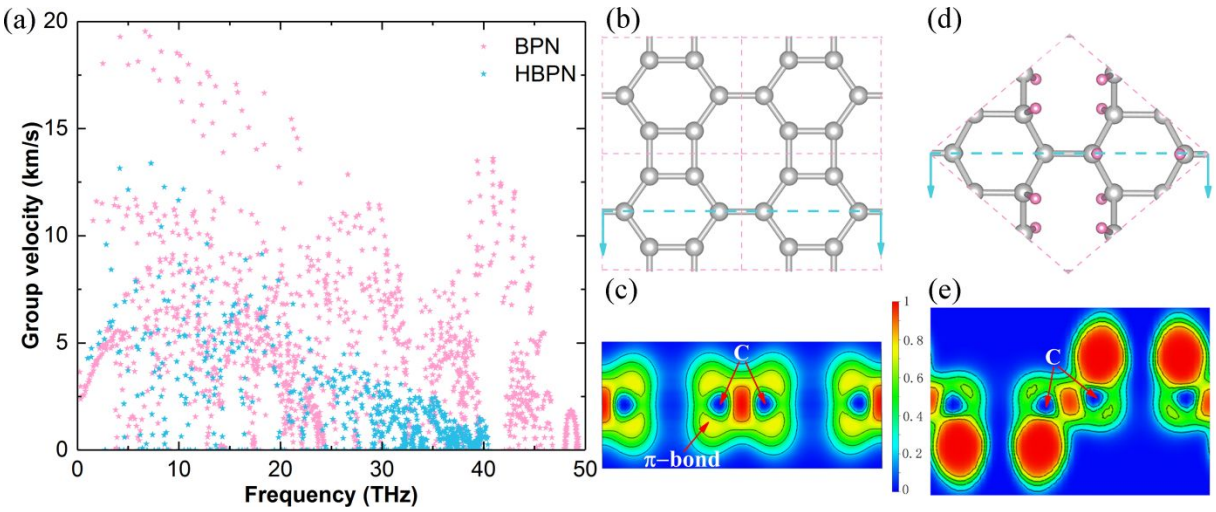

Figure 5. (a) Comparison of phonon group velocity of BPN and HBPN. (b, c) Atomic structures of BPN and HBPN, the blue dashed line indicates the cross section of the electron localization function (ELF). (d, e) ELF of BPN and HBPN. The two bonded carbon atoms are denoted by "C".

4. Conclusion

In summary, by combining the first-principles calculations with the Boltzmann transport theory, we systematically investigated the thermal transport properties of BPN and HBPN. Since higher-order phonon scattering plays an important role in more accurate calculations of the thermal conductivity of materials, four-phonon scattering is also considered in our work. The calculations show that the thermal conductivity of BPN decreases by 46.84% (57.05%) along the *x* (*y*) direction because of the increase in scattering rate, after considering the four-phonon scattering. Meanwhile, another important result indicates that hydrogenation not only weakens the anisotropy of thermal conductivity of BPN and phonon hydrodynamics of BPN, shortens the PMFP as well, but also leads

to a significant decrease in $\kappa_{\mathrm{avg}}^{3+4\,ph}$. At room temperature, the $\kappa_{\mathrm{avg}}^{3+4\,ph}$ of HBPN is merely 51.46 (54.73) W /mK, which is about 16.62% (10.14%) of that of BPN. Through analyzing phonon modes performance, one can find that both the phonon scattering rate and group velocity are responsible for the decrease of $\kappa_{\mathrm{avg}}^{3+4\,ph}$ after hydrogenation of BPN, which further attribution to the enlarged scattering phase space (including the 3-phonon and 4-phonons) and the weaker C-C bond. Our calculations shed light on the inherent phonon transport characteristics of BPN and the effect of hydrogenation, and provide theoretical guidance for potential applications of BPN and HBPN.

CRediT authorship contribution statement

Pei Zhang: Data curation, Formal analysis, Investigation, Visualization, Writing - original draft, Writing - review &editing, Funding acquisition. Tao Ouyang: Conceptualization, Methodology, Supervision, Validation, Funding acquisition, Writing - review & editing. Chao Tang: Resources, Software, Discussion, Writing - review & editing. Chaoyu He: Discussion, Writing- review & editing. Jin Li: Discussion, Writing - review & editing. Chunxiao Zhang: Discussion, Writing - review & editing. Ming Hu: Conceptualization, Validation, Discussion, Funding acquisition, Writing - review &editing. Jianxin Zhong: Discussion, Funding acquisition, Writing - review &editing.

Declaration of Competing Interest

The authors declare that they have no known competing financial interests or personal relationships that could have appeared to influence the work reported in this paper.

Acknowledgments

Project supported by the National Natural Science Foundation of China (Nos. 11974300, 11974299, 11704319), Natural Science Foundation of Hunan Province (2021JJ30645), Scientific Research Fund of Hunan Provincial Education Department (Nos. 20K127, 20A503, 20B582), Program for Changjiang Scholars and Innovative Research Team in University (IRT13093) and the Hunan Provincial Innovation Foundation for Postgraduate (No. CX20200624). Research reported in this publication was supported in part by the NSF (award number 2030128).

References

1. H. W. Kroto, J. R. Heath, S. C. O'Brien, R. F. Curl and R. E. Smalley, *Nature*, 1985, **318**, 162-163.
2. R. Baughman, H. Eckhardt and M. Kertesz, *The Journal of chemical physics*, 1987, **87**, 6687-6699.
3. S. Iijima, *Nature*, 1991, **354**, 56-58.
4. Y. P. Kudryavtsev, R. B. Heimann and S. E. Evsyukov, *J Mater Sci*, 1996, **31**, 5557-5571.
5. K. S. Novoselov, A. K. Geim, S. V. Morozov, D.-e. Jiang, Y. Zhang, S. V. Dubonos, I. V. Grigorieva and A. A. Firsov, *Science*, 2004, **306**, 666-669.
6. A. Hirsch, *Nature Materials*, 2010, **9**, 868-871.
7. Z.-S. Wu, W. Ren, L. Gao, J. Zhao, Z. Chen, B. Liu, D. Tang, B. Yu, C. Jiang and H.-M. Cheng, *ACS Nano*, 2009, **3**, 411-417.
8. L. Lindsay, D. A. Broido and N. Mingo, *Physical Review B*, 2010, **82**, 115427.
9. A. N. Enyashin and A. L. Ivanovskii, *physica status solidi (b)*, 2011, **248**, 1879-1883.
10. X.-Q. Wang, H.-D. Li and J.-T. Wang, *Physical Chemistry Chemical Physics*, 2013, **15**, 2024-2030.
11. W.-J. Yin, Y.-E. Xie, L.-M. Liu, R.-Z. Wang, X.-L. Wei, L. Lau, J.-X. Zhong and Y.-P. Chen, *J Mater Chem A*, 2013, **1**, 5341-5346.
12. X. Li, Q. Wang and P. Jena, *The Journal of Physical Chemistry Letters*, 2017, **8**, 3234-3241.
13. X. Wang, Z. Feng, J. Rong, Y. Zhang, Y. Zhong, J. Feng, X. Yu and Z. Zhan, *Carbon*, 2019, **142**, 438-444.

14. Q. Song, B. Wang, K. Deng, X. Feng, M. Wagner, J. D. Gale, K. Müllen and L. Zhi, *Journal of Materials Chemistry C*, 2013, **1**, 38-41.

15. S. Zhang, J. Zhou, Q. Wang, X. Chen, Y. Kawazoe and P. Jena, *Proceedings of the National Academy of Sciences*, 2015, **112**, 2372.

16. J.-W. Jiang, J. Leng, J. Li, Z. Guo, T. Chang, X. Guo and T. Zhang, *Carbon*, 2017, **118**, 370-375.

17. B. Wu, X. Jia, Y. Wang, J. Hu, E. Gao and Z. Liu, *J Mater Chem A*, 2019, **7**, 17357-17365.

18. C. Su, H. Jiang and J. Feng, *Physical Review B*, 2013, **87**, 075453.

19. Z. Wang, X.-F. Zhou, X. Zhang, Q. Zhu, H. Dong, M. Zhao and A. R. Oganov, *Nano Letters*, 2015, **15**, 6182-6186.

20. H. Yin, X. Shi, C. He, M. Martinez-Canales, J. Li, C. J. Pickard, C. Tang, T. Ouyang, C. Zhang and J. Zhong, *Physical Review B*, 2019, **99**, 041405.

21. Z. Gong, X. Shi, J. Li, S. Li, C. He, T. Ouyang, C. Zhang, C. Tang and J. Zhong, *Physical Review B*, 2020, **101**, 155427.

22. G. Li, Y. Li, H. Liu, Y. Guo, Y. Li and D. Zhu, *Chemical Communications*, 2010, **46**, 3256-3258.

23. Q. Fan, D. Martin-Jimenez, D. Ebeling, C. K. Krug, L. Brechmann, C. Kohlmeyer, G. Hilt, W. Hieringer, A. Schirmeisen and J. M. Gottfried, *Journal of the American Chemical Society*, 2019, **141**, 17713-17720.

24. Q. Fan, L. Yan, M. W. Tripp, O. Krejčí, S. Dimosthenous, S. R. Kachel, M. Chen, A. S. Foster, U. Koert and P. Liljeroth, *Science*, 2021, **372**, 852-856.

25. F. Q. Wang, J. Yu, Q. Wang, Y. Kawazoe and P. Jena, *Carbon*, 2016, **105**, 424-429.

26. P. H. Jiang, H. J. Liu, L. Cheng, D. D. Fan, J. Zhang, J. Wei, J. H. Liang and J. Shi, *Carbon*, 2017, **113**, 108-113.

27. M. Hu, K. P. Giapis, J. V. Goicochea, X. Zhang and D. Poulikakos, *Nano Letters*, 2011, **11**, 618-623.

28. W.-L. Ong, E. S. O'Brien, P. S. M. Dougherty, D. W. Paley, C. Fred Higgs Iii, A. J. H. McGaughey, J. A. Malen and X. Roy, *Nature Materials*, 2017, **16**, 83-88.

29. L. Yang, N. Yang and B. Li, *Nano Letters*, 2014, **14**, 1734-1738.

30. T. Ouyang, Q. Liu, M. Chen, C. Tang, J. Li, C. Zhang, C. He, H. Bao, J. Zhong and M. Hu, *ES Energy & Environment*, 2018, **3**, 88-95.

31. N. F. Hinsche, B. Y. Yavorsky, I. Mertig and P. Zahn, *Physical Review B*, 2011, **84**, 165214.

32. G. Qin, Z. Qin, H. Wang and M. Hu, *Nano Energy*, 2018, **50**, 425-430.

33. P. Zhang, T. Ouyang, C. Tang, C. He, J. Li, C. Zhang and J. Zhong, *Physica E: Low-dimensional Systems and Nanostructures*, 2020, **118**, 113870.

34. S.-K. Chien, Y.-T. Yang and C. o.-K. Chen, *Applied Physics Letters*, 2011, **98**, 033107.

35. X. Wu, V. Varshney, J. Lee, T. Zhang, J. L. Wohlwend, A. K. Roy and T. Luo, *Nano Letters*, 2016, **16**, 3925-3935.

36. P. E. Blöchl, *Physical Review B*, 1994, **50**, 17953-17979.

37. G. Kresse and D. Joubert, *Physical Review B*, 1999, **59**, 1758-1775.

38. J. Hafner, *Journal of computational chemistry*, 2008, **29**, 2044-2078.

39. J. P. Perdew, K. Burke and M. Ernzerhof, *Physical Review Letters*, 1996, **77**, 3865-3868.

40. A. Togo and I. Tanaka, *Scripta Materialia*, 2015, **108**, 1-5.

41. W. Li, L. Lindsay, D. A. Broido, D. A. Stewart and N. Mingo, *Physical Review B*, 2012, **86**, 174307.

42. Z. Han, X. Yang, W. Li, T. Feng and X. Ruan, *arXiv preprint arXiv:2104.04895*, 2021.

43. W. Li, J. Carrete, N. A. Katcho and N. Mingo, *Computer Physics Communications*, 2014, **185**, 1747-1758.

44. H. P. Veeravenkata and A. Jain, *Carbon*, 2021, **183**, 893-898.

45. X. Shi, C. He, C. J. Pickard, C. Tang and J. Zhong, *Physical Review B*, 2018, **97**, 014104.

46. Y. Liao, X. Shi, T. Ouyang, C. Zhang, J. Li, C. Tang, C. He and J. Zhong, *The Journal of Physical Chemistry Letters*, 2021, **12**, 8889-8896.

47. G. Xie, D. Ding and G. Zhang, *Advances in Physics: X*, 2018, **3**.

48. G. Xie, Z. Ju, K. Zhou, X. Wei, Z. Guo, Y. Cai and G. Zhang, *npj Computational Materials*, 2018, **4**.

49. P.-Z. Jia, Y.-J. Zeng, D. Wu, H. Pan, X.-H. Cao, W.-X. Zhou, Z.-X. Xie, J.-X. Zhang and K.-Q. Chen, *Journal of Physics: Condensed Matter*, 2019, **32**, 055302.

50. Y. Machida, N. Matsumoto, T. Isono and K. Behnia, *Science*, 2020, **367**, 309.

51. W. Kaim, B. Schwederski and A. Klein, *Bioinorganic Chemistry--Inorganic Elements in the Chemistry of Life: An Introduction and Guide*, John Wiley & Sons, 2013.